Bragg edge imaging characterization of multi-material laser powder-bed fusion specimens

F Malamud[1,2,] E Polatidis[1], M Busi[1], J. Capek[1], L Deillon[3], M Bambach[3], P Zehnder[3], A Losko[4], M Strobl[1]

[1]Paul Scherrer Institute, 5232 Villigen PSI, Switzerland, [2]LAHN, CONICET, Centro Atómico Bariloche, Av.Bustillo 9500, Bariloche, Argentina, [3] Advanced Manufacturing Laboratory, ETHZ, Technoparkstrasse 1, 8005 Zürich, Switzerland, [4]Technische Universität München, Lichtenbergstrasse 1, 85748 Garching, Germany

florencia.malamud@psi.ch

Abstract. Multi-material laser powder-bed fusion (M2LPBF) is a novel additive manufacturing approach that makes it possible to print different materials along the built direction and within a single layer of a component. At the interface between the different materials, the deposited powders melt, mix and solidify very rapidly, than can produce a range of desired and undesired phases, residual stresses and defects. Here we applied Bragg edge imaging to characterize M2LPBF specimens of stainless steel and CuCrZr with vertical and horizontal interfaces. A diffuse interface is observed in the samples with both vertical and horizontal interfaces. The analysis of the (111) and (200) Bragg edges height across the samples demonstrated a clear difference between the crystallographic texture of both alloys, with a strong alignment of the (002) planes along one of the transversal directions in the steel and a random texture within the copper alloy.

1. Introduction

In recent years, multi-material additive manufacturing has gained significant interest due to the high level of design freedom that it can offer, integrating structure and function to achieve tailored properties [1–3]. The latest progress in multi-material laser powder-bed fusion (M2LPBF), makes it possible to process at least two different materials along the built direction and within a single layer of a component [4]. At the interface between the different powder fractions, the deposited powders melt, mix and solidify very rapidly. This in-situ alloying process takes place far from equilibrium and can produce a range of desired and undesired phases, residual stresses, and defects [1]. The characterization of such microstructural features is a key aspect to understand the manufacturing process, optimizing the process parameters, and controlling the quality of the final part. Moreover, the increasing complexity of M2LPBF-built components demands advanced spatially-resolved characterization techniques to characterize the microstructure distribution with the corresponding three-dimensional spatial resolution. In this sense, Bragg edge imaging (BEI) holds great potential in spatially resolved studies of engineering materials and enables local crystallographic observations even in complex components [5]. Here we applied Bragg edge imaging to non-destructively characterize M2LPBF specimens of 316L stainless steel and CuCrZr alloy built with vertical and horizontal interfaces and different process parameters, employing the BOA beamline at PSI.

2. Samples

We have studied five M2LPBF layered specimens of austenitic stainless steel 316L and CuCrZr alloy with horizontal and vertical interfaces, employing two sets of process parameters. The starting raw materials were 316L stainless steel powder from Carpenter (16-18Cr, 10-12Ni, 2-3 Mo, <1Si, <1P, <1S, <0.05C, 5-25 μm) and CuCrZr from TLS Technik (0.5-1.2Cr, 0.03-0.3Zr, gas atomized, <32 μm). The bi-metallic structures were built using an Aconity Midi+ in combination with a newly developed recoater from Aerosint SA. The recoating unit allows for simultaneous local deposition of two powder materials with an in-plane resolution of 500x500 μm and a layer thickness of 40 μm. The structures were built onto a steel base plate kept at room temperature, always starting with a thin layer of 316L. Five samples were built with 100 μm hatch spacing and a rotation of 90° between successive layers. Figure 1 shows a schematic representation of the samples with different multimaterial arrangements in the same reference system: four bi-layered specimens with horizontal (Samples 1 and 2) and vertical interface (Samples 3 and 5) and a multi-layered specimen with horizontal interfaces (Sample 4). In all cases, the building direction (BD) is pointing vertically. The corresponding process parameters for the different samples are summarized in table 1, together with the corresponding volumetric energy density $E = P/_{v\,h\,t}$, where P is the laser power, v the scanning speed, h the hatch spacing and t the layer thickness [6]. For samples 1, 2 and 3, a remelting strategy was adopted for CuCrZr.
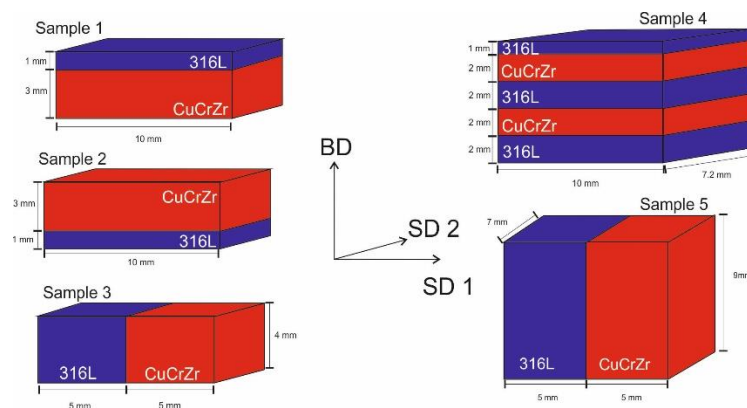

Figure 1. Schematic representation of the studied samples

Table 1. Processing parameters

| | Sample | Interface | Parameters | | E (J/mm^3) | | |
			CuCrZr	316L	CuCrZr	316L	
Set 1	1	Horizontal					Bi-layered: 316L on top of CuCrZr
	2	Horizontal	490W 550mm/s	150W 600mm/s	222.7	62.5	Bi-layered: CuCrZr on top of 316L
	3	Vertical					316L scanned first, CuCrZr scanned with a 100 μm offset into 316L
Set 2	4	Horizontal	350W 625mm/s	250W 900mm/s			Multi-layered
	5	Vertical			140	69.4	316L scanned first, CuCrZr scanned with a 250 μm offset into 316L

3. Bragg edge imaging experiments and data analysis

The Bragg edge imaging measurements were performed at the BOA beamline [7] at the Swiss spallation neutron source (SINQ) of the Paul Scherrer Institute (PSI) in Switzerland, employing the recently

developed Frame Overlap Bragg edge Imaging (FOBI) technique [8] using a TPX3CAM detector system for event-based neutron detection [9]. The FOBI technique is well suited for continuous neutron sources and uses a multiple slit chopper system to enable Bragg edge imaging with a higher duty cycle compared to a conventional single slit chopper disk. For this study, we used a chopper disk of 200 mm radius, with a pseudorandom angular distribution of 10 slits, repeated equally in 4 disk quadrants. The slit width was 1.8 mm and the rotation frequency 25 Hz, resulting in a wavelength resolution of ~1.1% $\Delta\lambda/\lambda$ at 1Å. The FOBI technique [8] was utilized to disentangle the pulse overlap produced by the multiple slits. The detector system was equipped with a 100 μm ^{6}LiF:ZnS scintillator positioned in the direct beam at 4.8 m distance to the chopper. Visible light coming from the scintillator was reflected with a mirror positioned at 45° relative to the scintillator, such that the TPXCAM could be positioned outside the direct beam. To adjust the focus onto the scintillator surface and amplify the light coming off the scintillator, a 100 mm lens was coupled with a dual stage image intensifier. The optical setup provided a field-of-view of 10 cm × 10 cm with an effective pixel size of 90 μm.

The measurements comprised a set of imaging acquisitions of the samples, with the neutron beam along the SD1 and SD2 for samples 1, 2 and 4, with horizontal interfaces, and along the BD and SD2 directions for the samples with vertical interface (samples 3 and 5). For each measurement, the samples were exposed for 20 hs in radiography mode, preceded by an open beam exposure of 10 hs and a pure iron powder measurement of 6 hs for calibration. The data were analyzed pixel by pixel employing the FOBI retrieval method and the signal processing algorithms presented in [8], with the corresponding chopper time delay scheme. After the FOBI retrieval, the time-of-flight to neutron wavelength calibration was performed by fitting the (110), (200) and (311) Bragg edges of a BCC iron powder standard with well-known lattice parameters, employing a non-linear function for the edge profile [10].

4. Results and discussion

The transmission images averaged along the $[2-4.5]$Å wavelength range with the beam along the SD2 direction are shown in Figure 2-a for samples of set 1 (samples 1,2 and 3) and in Figure 2-c for samples of set 2 (samples 4 and 5). A clear contrast is observed between the 2 constitutive materials in all samples, due to the different attenuation coefficients of the copper and steel alloys, allowing a straightforward identification of the interface. The transmission intensity changes across the samples and among the same material imply the presence of defects, as cracks or porosity, or intermixing regions. In particular for samples 4 and 5, optical microscopy analysis allowed the correlation of the regions with increasing transmission in CuCrZr areas with porosity effects, with pore sizes varying from 1 to 150 μm, and allows the identification of cracks along the interfaces and more specifically on the 316L side in sample 5. Those samples presented more porosity at the CuCrZr regions than samples 1,2 and 3 due to the lower energy input employed during the building process, which results in numerous lack-of-fusion defects. The presence of pores and cracks at the interfaces of steel and copper alloys built by LPBF with horizontal interface was also reported by other authors [11–13]. The presence of cracks in the steel region can be related to the build-up of strong residual stresses arising from the mismatch in thermal and elastic properties between the two alloys [12], combined to the susceptibility of 316L to a type of liquid metal embrittlement known as copper contamination cracking [14,15]

The corresponding transmission signals after the FOBI retrieval for the different phases and regions of the samples printed with parameters of set 1 and 2 are shown in Figure 2-b and Figure 2-d respectively, in red for the CuCrZr alloy and blue for 316L. In all cases, the Bragg edges corresponding to the FCC crystal lattice structures of both alloys are indexed. The transmission spectra exhibit the same Bragg edges for all the samples, with similar positions, considering that both alloys present the same crystal structure with similar lattice parameters (~ 3.6 Å), but different heights due to the preferential crystallographic orientation, i.e. texture, along the neutron beam direction. To characterize the samples interfaces, we analyzed the average transmission signal for wavelengths larger than the (111) Bragg edge ($\lambda > 4.17$), where no texture effects are present and only the absorption and thermal diffuse

scattering components of the neutron attenuation coefficient contribute to the transmission intensity for samples with constant thickness.
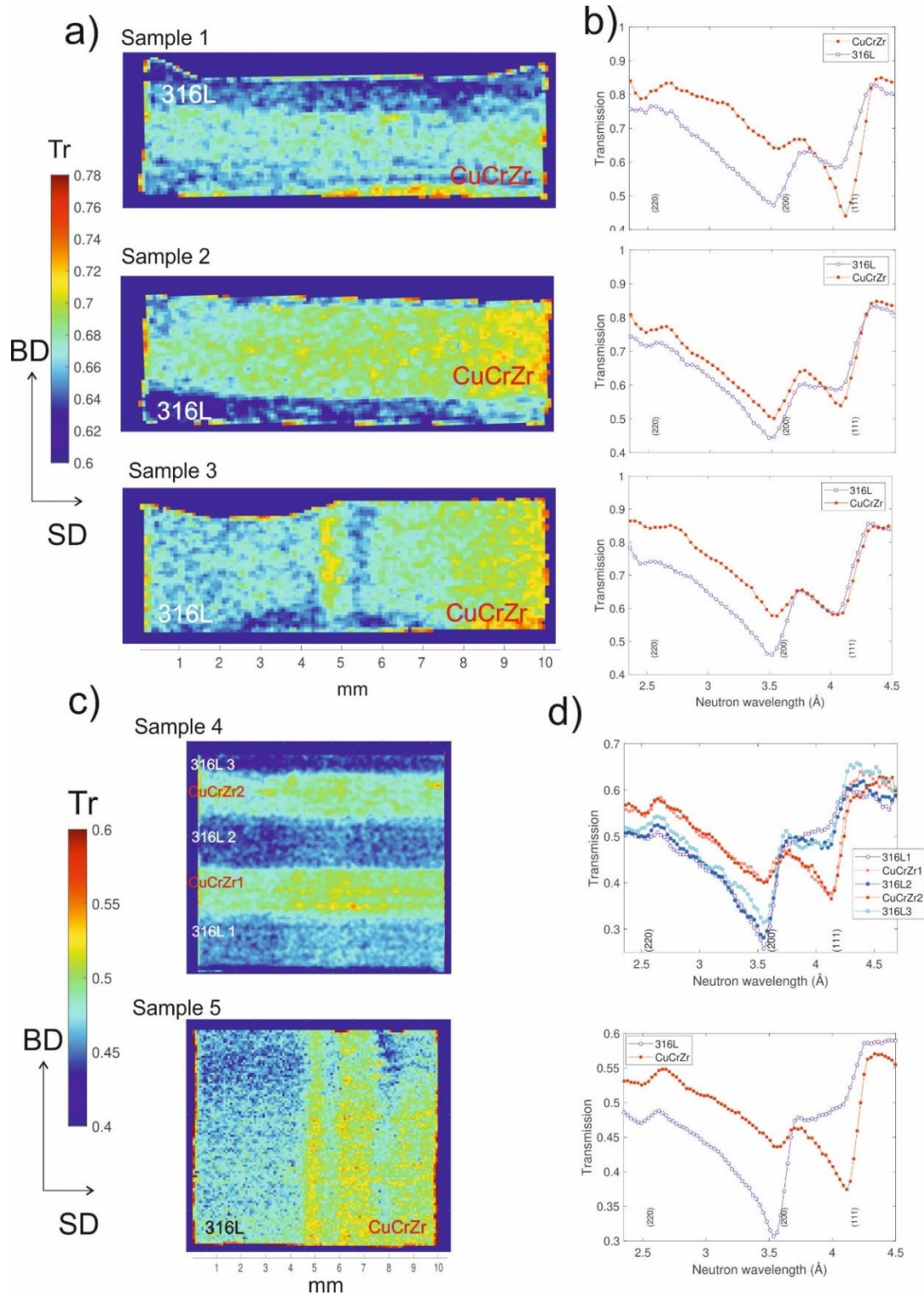

Figure 2. Transmission images along the SD1 neutron beam direction averaged along the $[2 − 4.5]$Å wavelength range in the same color scale of samples 1, 2 and 3 (a) and of samples 4 and 5 (c), and

FOBI retrieved transmission signal of samples 1, 2 and 3 (b) and samples 4 and 5 (d), obtained at the CuCrZr and 316L interface

Figure 3 shows the average transmission value within the wavelength range of $4.17 - 4.55$ Å centered at the samples interface for samples 1 and 2 (Figure 3-a) and sample 3 (Figure 3-b). It is observed that the interdiffusion region, corresponding to a gradient in transmission, across the sample with horizontal interface is smaller than across the sample with vertical interface. The obtained interdiffusion region thicknesses for the different interfaces are listed in Table 2. In particular, the intermixing region of sample 2, where CuCrZr was built on top of 316L displays a wider interface than sample 1, where 316L was built on top of CuCrZr. The same behavior was observed for the samples of setup 2, showing a wider interface for the sample with vertical interface (sample 5), than the diffusion regions of the multi-layered sample. Similar results were found by EDX analysis across the sample interfaces. The wider interface when CuCrZr is printed on top of 316L was also observed by Liu and collaborators in a 316L/CuSn10/316L multi-layered sample with horizontal interphase [12] and can be explained by the higher energy needed to melt CuCrZr, which leads to the formation of deeper melt pools and more remelting of the underlying 316L. On the other hand, when 316L is printed on top of CuCrZr, the lower laser power and high scanning speed result in relatively low VED, which in combination with the rapid heat dissipation of the copper results in shallower melt pools. This melt pool geometry presents a smaller penetration depth at the pre-printed copper layer, leading to a thinner interdiffusion zone.
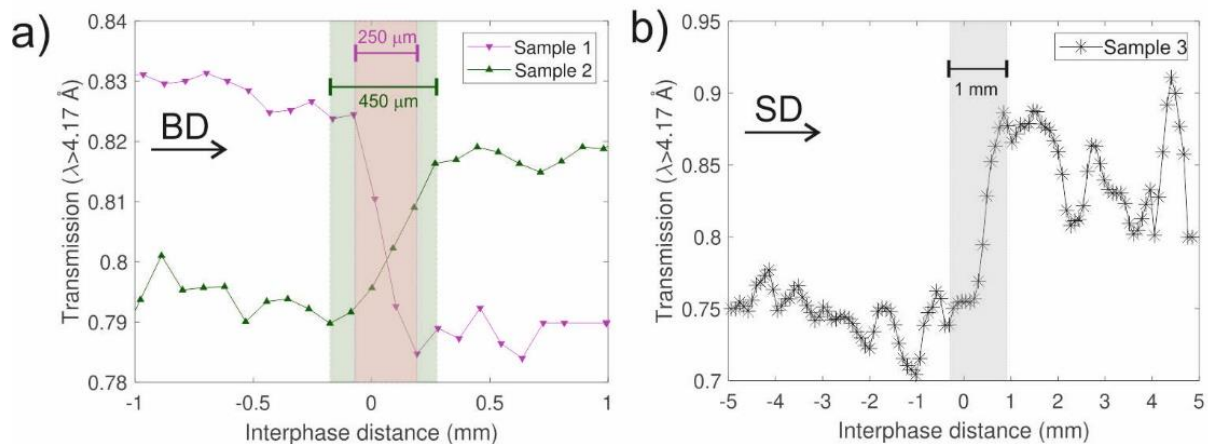

Figure 3. Transmission intensities profiles averaged along the $[4.17 - 4.5]$Å wavelength range for samples 1 and 2 (a) and sample 3 (b)

Table 2: Diffusion region thickness

Sample	Diffusion region thickness (μm)	
1	250	
2	450	
3	1000	
4	316L1/CuCrZr1	350
	CuCrZr1/316L2	210
	316L2/CuCrZr2	400
	CuCrZr2/316L3	250
5	900	

By comparing the (111) and (200) Bragg edge heights of the samples with the ones expected for a crystallographic random-oriented material, it is possible to characterize the crystallographic texture variation of the samples. For all samples, the 316L layers display a strong alignment of the (200) planes along the SD1, while the CuCrZr layers display nearly random crystallographic texture. In particular, for the samples with horizontal interfaces, a similar crystallographic texture trend was found on the transmission signal corresponding to the neutron beam along the SD2, which is consistent with the building parameters and scanning strategy of a 90° rotation per layer. For samples 1 and 2, the height of the (200) Bragg edge of the 316L layers is different when the 316L is built first or on top of CuCrZr. This behavior was also observed in sample 4, as it is shown in Figure 4-a, where the profile of the height of the (111) and (200) Bragg edges is plotted as a function of the distance to the building plate. The crystallographic texture variation of the multi-layered sample was also characterized by EBSD, confirming the same behavior observed by Bragg edge imaging. Figure 4-b shows the inverse pole figure in the SD2 direction obtained by the EBSD maps located at the center of each layer, in the same scale, which confirms the strong <001> texture in 316L and the nearly random crystallographic texture in CuCrZr.
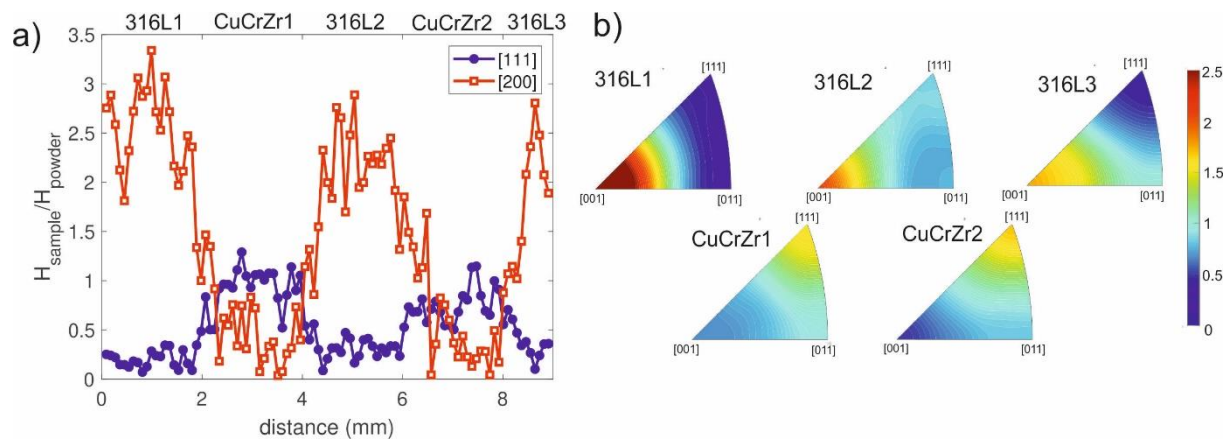

Figure 4. Sample 4: a) H_{sample}/H_{powder} profile of the (111) and (200) Bragg edges as a function of the distance to the building plate, where H_{sample} and H_{powder} are the Bragg edge height of the sample and expected for a crystallographic random-oriented material respectively, b) Inverse pole figures in the SD2 direction for the different layers

5. Conclusion

We have performed a Bragg edge imaging characterization of 316L and CuCrZr specimens built with M2LPBF with horizontal and vertical interfaces. The transmission images allowed the identification of defects, such as porosity and cracks along the interface. The transmission spectra analysis after the (111) Bragg edge enabled the characterization of the diffusion zone at the interface, while the Bragg edge height analysis was employed to analyze crystallographic texture variations across the samples. The results display an excellent agreement with conventional microstructure characterization techniques, such as EBSD, and can be linked with the building parameters, demonstrating the capabilities of Bragg edge neutron imaging for efficient non-destructive characterization of multi-materials built by LPBF.

References

[1]   Wei C, Zhang Z, Cheng D, Sun Z, Zhu M and Li L 2020 *Int. J. Extrem. Manuf.* **3** 012003

[2]   Binder M, Anstaett C, Horn M, Herzer F, Schlick G, Seidel C, Schilp J and Reinhart G 12

[3]   Wei C, Li L, Zhang X and Chueh Y-H 2018 *CIRP Annals* **67** 245–8

[4]   Walker J, Middendorf J R, Lesko C C C and Gockel J 2022 *Manufacturing Letters* **31** 74–7

[5]   Woracek R, Santisteban J, Fedrigo A and Strobl M 2018 *Nuclear Instruments and Methods in Physics Research Section A: Accelerators, Spectrometers, Detectors and Associated Equipment* **878** 141–58

[6]   Sing S L and Yeong W Y 2020 *Virtual and Physical Prototyping* **15** 359–70

[7]   Morgano M, Peetermans S, Lehmann E H, Panzner T and Filges U 2014 *Nuclear Instruments and Methods in Physics Research Section A: Accelerators, Spectrometers, Detectors and Associated Equipment* **754** 46–56

[8]   Busi M, Čapek J, Polatidis E, Hovind J, Boillat P, Tremsin A S, Kockelmann W and Strobl M 2020 *Scientific Reports* **10** 14867

[9]   Losko A S, Han Y, Schillinger B, Tartaglione A, Morgano M, Strobl M, Long J, Tremsin A S and Schulz M 2021 *Sci Rep* **11** 21360

[10]   Santisteban J R, Edwards L, Steuwer A and Withers P J 2001 *Journal of Applied Crystallography* **34** 289–97

[11]   Chen J, Yang Y, Song C, Wang D, Wu S and Zhang M 2020 *Materials Science and Engineering: A* **792** 139316

[12]   Liu L, Wang D, Deng G, Yang Y, Chen J, Tang J, Wang Y, Liu Y, Yang X and Zhang Y 2022 *Chinese Journal of Mechanical Engineering: Additive Manufacturing Frontiers* **1** 100045

[13]   Liu Z H, Zhang D Q, Sing S L, Chua C K and Loh L E 2014 *Materials Characterization* **94** 116–25

[14]   Rao S and Al-Kawaie A Y 2010 *Welding Journal*

[15]   Savage W F, E.P.NIPPESANDM C and Mushala 2013